Polarization-dependent absorption in Ge/SiGe multiple quantum wells: Theory and experiment

Michele Virgilio,[1] Matteo Bonfanti,[2,*] Daniel Chrastina,[3] Antonia Neels,[4] Giovanni Isella,[3] Emanuele Grilli,[2] Mario Guzzi,[2] Giuseppe Grosso,[1] Hans Sigg,[5] and Hans von Känel[3]

[1]*Dipartimento di Fisica "E. Fermi" and CNR-NEST-INFM, Università di Pisa, Largo Pontecorvo 3, I-56127 Pisa, Italy*

[2]*Dipartimento di Scienza dei Materiali and L-NESS, Università degli Studi di Milano-Bicocca, Via Cozzi 53, I-20125 Milano, Italy*

[3]*Dipartimento di Fisica and L-NESS, Politecnico di Milano, Polo di Como, via Anzani 42, I-22100 Como, Italy*

[4]*Institute of Microtechnology, University of Neuchâtel, Rue Jaquet-Droz 1, CH-2002 Neuchâtel, Switzerland*

[5]*Laboratory for Micro- and Nanotechnology, Paul Scherrer Institut, CH-5232 Villigen-PSI, Switzerland*

(Received 14 November 2008; revised manuscript received 27 January 2009; published 25 February 2009)

Polarization resolved absorption spectra of a strain-compensated Ge multiple quantum well (MQW) structure with Ge-rich SiGe barriers have been calculated with an $sp^3d^5s^*$ tight-binding model and measured for light propagating perpendicular to the growth direction. The MQW was grown by low-energy plasma-enhanced chemical vapor deposition and consists of 50 Ge quantum wells deposited onto a thick graded $Si_{1-x}Ge_x$ buffer layer. The MQW was structurally characterized by high-resolution x-ray diffraction. The measured absorption spectra show clear quantum confined excitonic transitions related to the Ge Γ point band gap, and strong dependence on the incident light polarization, as expected from selection rules for type I direct gap quantum confined systems. A good agreement between theoretically predicted spectra and experimental data is found, demonstrating light and heavy hole polarization-dependent selection rules in Ge MQWs.

DOI: 10.1103/PhysRevB.79.075323 PACS number(s): 73.21.Fg, 78.67.De

I. INTRODUCTION

Understanding of the electronic properties of semiconductor quantum-confined structures is a key requirement for the development of their potential applications in electronic and photonic devices. This is particularly relevant for heterostructures based on the SiGe system, in view of their compatibility with Si technology.

Most of the previous work concerning the optical properties of $Si_{1-x}Ge_x$ heterostructures was based on quantum wells (QWs) in SiGe alloys with relatively low Ge molar fraction ($x < 0.30-0.50$) (Refs. 1–7): this was motivated by the difficulty of growing strained Ge-rich heterostructures on Si substrates.[8] However, low-energy plasma-enhanced chemical vapor deposition (LEPECVD) (Ref. 9) has enabled the growth of high-quality Ge-rich heterostructures.[10–12] The interest in Ge-rich QWs is motivated by the fact that their optical properties are expected to exhibit close analogies to those of quantum-confined systems based on direct-gap semiconductors, because of the direct minimum in the conduction band at the Γ point which in Ge bulk is only 136 meV above the indirect minimum at the L point.[13]

The interest in SiGe-based QWs is also motivated by the fact that the type I band alignment, which characterizes the Γ states in this system, has important implications for Si-based photonics,[14–16] spintronics,[17] and quantum computing.[18] In particular, the quantum confined Stark effect[19] related to direct gap transitions at about 1.5 μm has been demonstrated in Ge multiple quantum wells (MQWs).[16,20]

Optical transitions and electronic states in Ge/SiGe MQWs with high Ge content barriers have recently been studied.[11,21,22] In particular, quantum-confined transitions related to the direct gap at the Γ point of Ge were discussed,[21] using high-resolution absorption and photoluminescence spectra and high-resolution x-ray diffraction (HRXRD), combined with tight-binding calculations which are known to be very efficient in treating band alignment as well as inter- and intra-subband transitions in SiGe multilayer structures.[23]

Polarization-dependent selection rules have been predicted and experimentally demonstrated for III-V semiconductor QWs.[24–26] In this paper we present a detailed study of the polarization dependence of the absorption coefficient in Ge/SiGe MQWs with high Ge content barriers. The absorption was measured for linearly polarized light propagating in the MQW plane and the spectra were compared with those calculated by a tight-binding model. Thickness, strain state, and Ge content of the SiGe MQWs were determined by HRXRD; system geometry and Ge content of buffer, barrier, and well are used as input parameters for the calculations. A good agreement has been found between theoretically predicted spectra and experimental data.

The paper is organized as follows. In Sec. II we describe the investigated MQW sample and the experimental methods adopted; in Sec. III we introduce the tight-binding model exploited to describe the electronic states and the optical absorption in the MQW system. As a guideline for the experimental and tight-binding data some elementary results for the polarization dependence of the optical absorption are also reported. Absorption spectra calculated by tight binding for unpolarized and polarized incident light are compared to measured spectra in Sec. IV. Section V contains our conclusions.

II. EXPERIMENTAL DETAILS

The heterostructure was grown by LEPECVD on a 100 mm Si(100) substrate with resistance of 1–10 Ω cm. The first part of the structure is a buffer graded from Si to $Si_{0.131}Ge_{0.869}$, over a thickness of 13 μm, and then capped with a 2 μm $Si_{0.131}Ge_{0.869}$ layer. This forms a fully relaxed virtual substrate (VS). The MQW system, shown in Fig. 1(a),

 ©2009 The American Physical Society

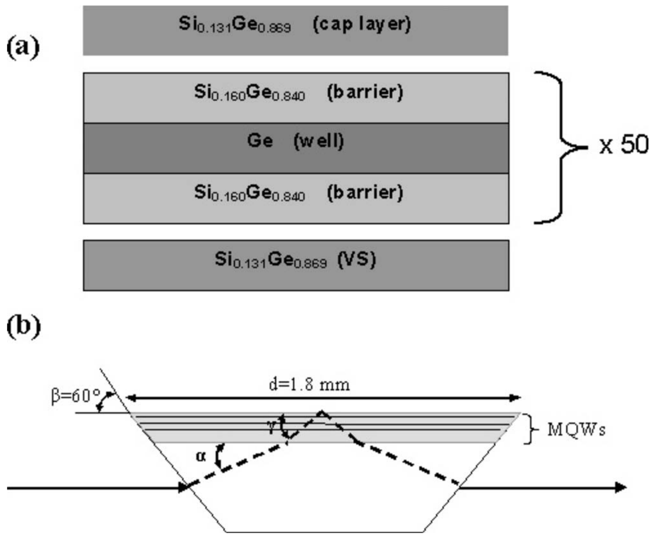

FIG. 1. (a) Layer stack of the MQW structure; (b) shape of the processed MQW sample (not to scale): the arrows show the optical path of the transmitted light. The angles α and γ are 22° and 37°, respectively (see text).

features 50 Ge QWs with $Si_{0.160}Ge_{0.840}$ barriers in between. Individual layer thicknesses were designed in order to balance the compressive strain in the QWs with the tensile strain in the barriers and obtain nominally zero net strain. The actual well and barrier thicknesses and the VS and barrier compositions were measured by high-resolution x-ray diffraction. The total growth time (including graded buffer) was limited to about 45 min by making use of the high deposition rates (4–6 nm s^{-1}) possible with LEPECVD.

The actual QW and barrier thicknesses and the VS and barrier compositions were obtained by HRXRD. These measurements were carried out with a PANalytical X'Pert PRO diffractometer using a Goebel mirror and a Bartels four-crystal monochromator on the primary beam path, and a triple crystal analyzer in front of a proportional x-ray detector. High-resolution $\omega-2\theta$ scans and reciprocal space mapping were performed in the vicinity of the (004) and (115) reflections. The results of these measurements, shown in Table I, confirm that the graded buffer is fully relaxed and that the MQW is fully lattice-matched to the top of the buffer.

The optical transmission measurements were performed at 5 and 300 K using a halogen light bulb and a Bruker Fourier transform spectrometer. The measured optical density (OD) is defined as $\mathrm{OD}(\lambda)=-\log_{10}[I_{TS}(\lambda)/I_0(\lambda)]$, where $I_{TS}(\lambda)$ and $I_0(\lambda)$ are the intensity of the transmission spectrum with or without the sample in the light pass. The measured spectra have been translated to OD=0.0 in the transparent region in order to compensate for reflection losses.

The sample was processed into a prism shape, as shown in Fig. 1(b), which also shows the optical path in the sample. The length d of the major basis of the prism is 1.8 mm and its angle β with the lateral facets is 60°. The incident light is refracted on entering the silicon substrate, propagates through it at a shallow angle α of about 22° with respect to the prism major basis, and is totally reflected after propagation through the MQW region. Before reaching the MQWs, the light is also refracted by the VS. We can estimate this refraction using the refractive index of Si ($n_{Si}=3.487$) and of $Si_{0.1}Ge_{0.9}$($n_{SiGe}=4.063$) at 1.5 μm (Ref. 27). We conclude that light propagates in the heterostructure at an angle γ of about 37° with respect to the prism basis.

The incident light is linearly polarized either in the QW plane (i.e., s or TE polarized) or perpendicular to it (i.e., p or TM polarized). Due to the geometry of the experiment, for the TE mode the electric field vector in the active region is parallel to the QW plane. For the TM mode both perpendicular $E_\perp$ and parallel $E_\parallel$ components of the electric field are present with $E_\perp=E_0\cos(\gamma)>E_\parallel=E_0\sin(\gamma)$.

TABLE I. Structural characteristic of the Ge MQW sample studied in this work as obtained from x-ray analysis.

	x	Thickness (nm)	In-plane strain
VS	0.869		
Well	1.000	17.0	–0.58%
Barrier	0.840	22.5	0.13%

III. TIGHT-BINDING MODEL AND OPTICAL SELECTION RULES FOR POLARIZED LIGHT

In this section we give a short description of the tight-binding model used to evaluate electronic states and optical absorption of the SiGe MQW sample described in Fig. 1(a). We simulate the QW and barrier regions of the structure, assuming infinite extension in the QW plane, periodic boundary conditions along the growth direction, and sharp and flat interfaces. In the chosen atomistic description, ion positions in each layer of the MQW are calculated matching the in-plane lattice constant with the relaxed $Si_{0.131}Ge_{0.869}$ VS and evaluating the monolayer positions along the growth direction by means of macroscopic elasticity theory.[23] The geometrical and chemical input data to describe the barrier and active materials have been taken from the measured values given in Table I.

The electronic structure of the system is investigated by means of a first-neighbor tight-binding Hamiltonian with $sp^3d^5s^*$ orbitals and spin-orbit interaction. The self and hopping energy parameters of the matrix Hamiltonian were obtained by Jancu *et al.*[28] to reproduce the electronic band structure of bulk silicon and germanium crystals. Linear interpolation of the Si and Ge tight-binding parameters (the virtual crystal approximation) is here exploited to describe the $Si_{0.160}Ge_{0.840}$ barriers. Strain effects are accounted for by the scaling laws given in Ref. 28 and by evaluation of the appropriate modification of the geometrical phase factors in the matrix Hamiltonian. To model the potential discontinuity at the heterointerfaces between the QW and barrier regions, we align their topmost valence band edges by adding a constant potential to the on-site self-energies in the QW region. The valence band offset is evaluated by linear interpolation with the Ge fraction x of the results reported in Ref. 29 for pristine Si/Ge heterointerfaces under different strain conditions.

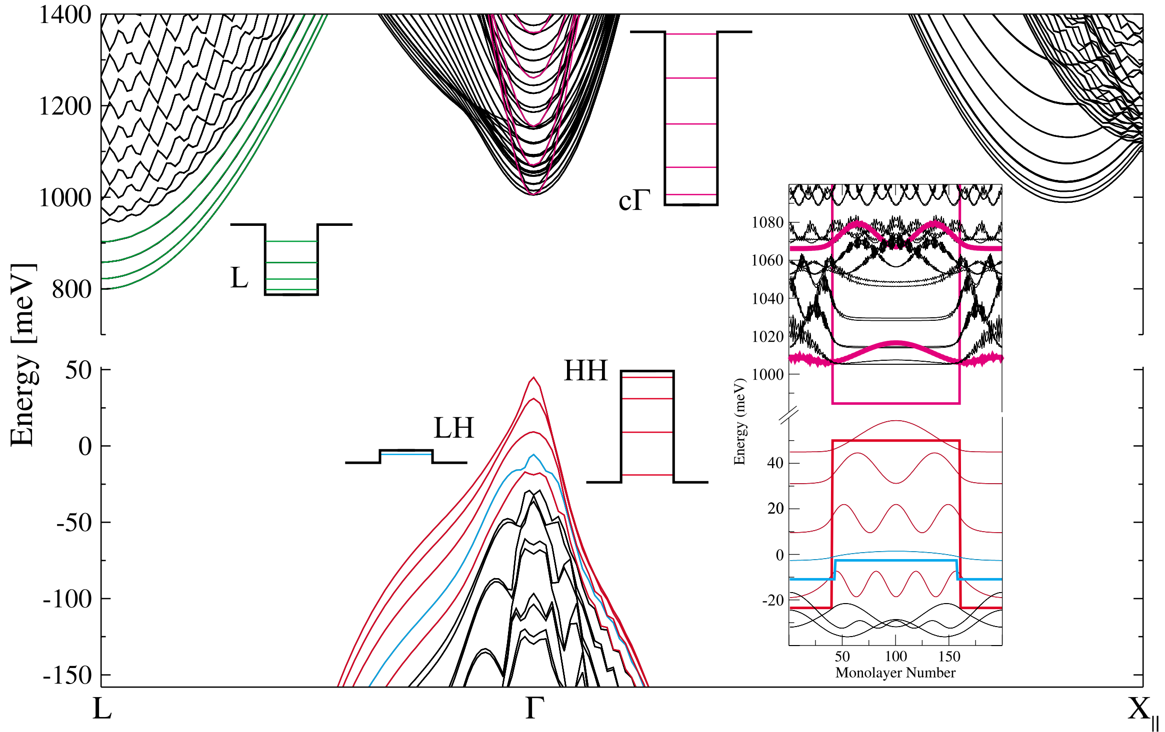

FIG. 2. (Color online) Calculated band structure for the system discussed in the text. QW conduction subbands close to the L and Γ points are reported in green and violet, respectively. Subbands in the valence band are shown in red (heavy hole) and blue (light hole). The bulk band edge profiles, evaluated for the strained Ge and SiGe materials, are sketched together with the energies of the MQW states at the L and Γ points. In the inset the square modulus of the wave functions of the near-gap electron and hole states are shown. Folded states (black, see text) are present in the conduction band near the Γ point.

The adopted tight-binding Hamiltonian provides a complete description of the electronic structure of the MQW system through the whole Brillouin zone (BZ); the near-gap bands are shown in Fig. 2. As expected from the obtained valence and conduction band alignments between strained Ge QWs and $Si_{0.160}Ge_{0.840}$ barriers (sketched profiles in Fig. 2), we find QW states confined in the Ge region. The lowest confined states in the conduction band are found at the L point (green subbands in Fig. 2). Confined states at the Γ point have higher energies and are shown in violet; in the same energy region, a large number of conduction states are also present (shown in black). As discussed in Ref. 23, these Γ states are due to the folding of the $\Delta_\perp$ line into the Γ point of the quasi-2D MQW BZ. These states are not genuine Γ states and our calculations indicate that their dipole matrix element with Γ valence band states is very small so that they remain optically inactive. Confined states in the valence band at Γ originate from heavy and light hole bands and are indicated in Fig. 2 in red and blue, respectively.

The spatial extension of the states can be inspected by projection of the system eigenfunctions onto each layer of the sample. Also, the symmetry of the states can be obtained by orbital and layer resolved projection.[30] As an example, the projected square modulus of the wave functions calculated at the Γ point is shown in the inset of Fig. 2 in which genuine Γ point conduction band states (i.e., not related to $\Delta_\perp \rightarrow \Gamma$ folding) have been shown as violet lines.

Interband optical absorption for polarized incident light is evaluated in the dipole approximation sampling the BZ close to the Γ point. This BZ sampling guarantees that nonparabolicity effects and $\vec{k}_\parallel$ dependence of the dipole matrix element are taken into account. Also, excitonic effects have been included in the model as explained in Ref. 23: the single-particle interband absorption is modified exploiting the two-dimensional Elliott formula[31] to describe the excitonic contributions below (Rydberg-type) and above (Coulomb enhancement) the interband gaps.

Before comparing the evaluated absorption spectrum with the measurements obtained for incident polarized light, it is convenient to briefly recall some elementary results for interband transitions between QW states in the envelope function approximation. These results can be used as a guideline to interpret the more accurate tight-binding numerical data and the experimental measurements presented in Sec. IV.

In the effective mass framework, the dipole matrix element d_{if} between states i and f can be approximated by[32]

$$d_{if} = \vec{\varepsilon} \cdot \vec{p}_{if} \cong \vec{\varepsilon} \cdot \int_{\Omega_0} u_{v_i}(r)\vec{p}u_{v_f}(r)d^3r \int_{\Omega} f_i^* f_f d^3r + \delta_{v_i v_f}\vec{\varepsilon} \cdot \int_{\Omega} f_i^* \vec{p} f_f d^3 r, \quad (1)$$

where $\vec{\varepsilon}$ is the polarization vector, $\vec{p}_{if}$ is the transition dipole moment, u_{v_i} and u_{v_f} are the periodic parts of the Bloch functions at Γ, f_i and f_f are the envelope functions, and Ω and Ω_0 are the sample and elementary cell volumes, respectively. For interband transitions the second term on the right-hand

side of Eq. (1) is negligible and selection rules related to the direction of the polarization vector are governed by the atomiclike term $\langle u_{v_i}|\vec{p}|u_{v_f}\rangle$. Further selection rules are connected to the overlap integral involving the envelope functions and do not depend on the incident light polarization. For instance, in the infinite wells approximation, the overlap term is not negligible only if the involved states have the same subband index. In effect the measured excitonic features discussed in the next section correspond to HH$n\rightarrow c\Gamma n$ and LH$n\rightarrow c\Gamma n$ transitions.

In the determination of interband $\vec{\varepsilon}$-dependent selection rules, contributions to the $\langle u_{v_i}|\vec{p}|u_{v_f}\rangle$ term arising from the mixing of the heavy hole (HH) ($m=\pm 3/2$) and light hole (LH) ($m=\pm 1/2$) states in the starting valence state $|u_{v_i}\rangle$ can be ignored. In fact, close to the Γ point this mixing is linear in $k_{\parallel}$ and in the strain tensor. Therefore, near the band edge and for moderate strain fields as in the case of the investigated SiGe sample, the correction to the dipole matrix element due to the HH-LH mixing is negligible (for a deeper discussion, see, for instance, Ref. 33). Then, the $c\Gamma$, HH, and LH bulk states close to the Γ point can be roughly described as J-decoupled states with parabolic dispersion. Within this approximation one finds that for a polarization vector in the QW plane, the HH$\rightarrow c\Gamma$ and LH$\rightarrow c\Gamma$ transitions are both allowed, and the absolute value of the dipole matrix elements for HH$\rightarrow c\Gamma$ is greater by a factor $\sqrt{3}$ with respect to the LH$\rightarrow c\Gamma$ transition. One can also verify that if the polarization vector is along the growth direction, the strength of the LH$\rightarrow c\Gamma$ transition is unchanged while the HH$\rightarrow c\Gamma$ transition becomes forbidden. This implies that for polarized light propagating parallel to the QW plane and polarization vectors along the growth direction the HH$n\rightarrow c\Gamma n$ transitions are expected to be strongly suppressed.

IV. ABSORPTION SPECTRA FOR POLARIZED LIGHT

Before discussing polarization-dependent effects, we report in Fig. 3 the near-edge transmission spectra measured with unpolarized light at 5 and 300 K, together with the low temperature absorption coefficient calculated with the tight-binding model. The direct gap energy at 5 K of relaxed bulk Ge is also shown for reference. The low temperature spectrum shows the typical staircase lineshape proportional to the joint density of states in direct-gap type I QWs, with narrow excitonic structures at the edges of each step. In fact, as demonstrated in Refs. 11, 16, and 20, the near-edge absorption spectrum of Ge-rich QWs is dominated by excitonic transitions involving heavy hole and light hole valence band states and conduction band states at the Γ point, spatially confined by a type I profile.

In the same spatial region, L point conduction band states are also present. They have lower energy with respect to the conduction band states at Γ. Nevertheless, the role of L states in the near-edge absorption region can be neglected due to the low oscillator strength related to the k-indirect nature of the Γ-L transitions. Therefore, by means of the tight-binding model, and in agreement with the selection rules summarized in Sec. III, we assign the experimental features shown in Fig. 3 to dipole-allowed transitions between valence band quantum-confined heavy hole (HHn) or light hole (LHn) subbands and conduction band subbands ($c\Gamma m$) with $n=m$.

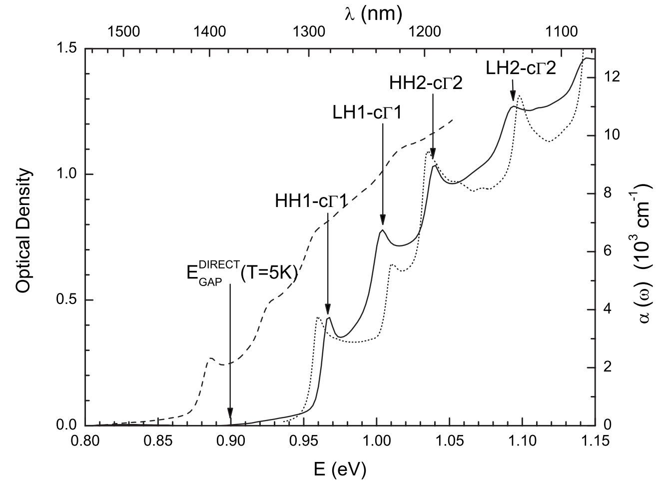

FIG. 3. Transmission spectra of the MQW sample measured at 300 K (dashed line) and at 5 K (full line) with unpolarized light (left-hand y axis). The prism configuration of Fig. 1(b) was adopted. The low temperature tight-binding theoretical absorption coefficient (dotted line) is also reported (right-hand y axis). The arrows indicate the HHn-$c\Gamma n$ and LHn-$c\Gamma n$ transitions; the low temperature bulk Ge direct gap energy is also reported for reference.

Low temperature measured OD for TE and TM polarizations of the incident radiation and the corresponding tight-binding absorption coefficients are shown in Fig. 4. The attribution of the peaks reported in Fig. 3 is here confirmed: the heavy hole related transitions (HH1-$c\Gamma$1 and HH2-$c\Gamma$2) are partially suppressed in the TM mode, whereas the peaks related to light hole transitions (LH1-$c\Gamma$1 and LH2-$c\Gamma$2) are almost unaffected by the polarization, as predicted by the selection rules.

Figure 4 shows that the OD of the HH1-$c\Gamma$1 exciton transition is reduced from $\mathrm{OD}^{\mathrm{TE}}=0.63$ for TE polarization to

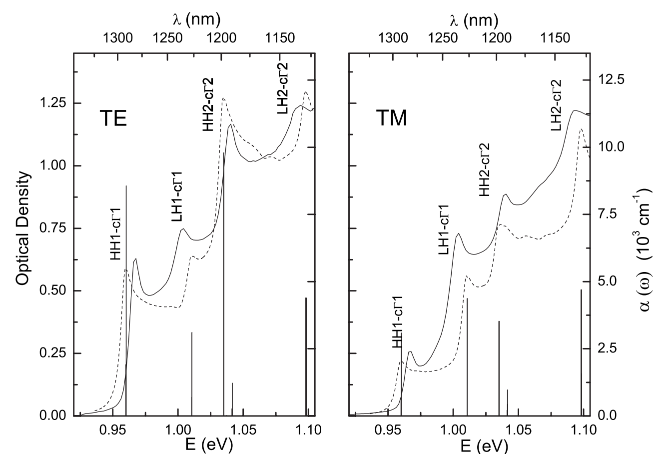

FIG. 4. Low temperature measured OD (solid line) and tight-binding theoretical absorption spectra (dashed line) in TE (left-hand panel) and TM (right-hand panel) polarization. Vertical lines represent, in arbitrary units, the square modulus of the dipole matrix elements calculated between near gap valence and conduction states at the Γ point. The weak transition at about 1.04 eV (not labeled) involves the SO1 and $c\Gamma$1 states.

$OD^{TM}=0.26$ for TM polarization, but it does not disappear completely as expected for pure TM polarization. This is due to the geometry of our experiment, as shown in Fig. 1(b): the TM mode includes a minor component, proportional to $\sin^2(\gamma)$, with TE character. The ratio between the peaks of the ODs in the two polarizations is $OD^{TM}/OD^{TE}=0.41$, which compares well with $\sin^2(\gamma)=0.36$.

In Sec. III it has also been shown that in the TE mode the dipole matrix elements of $HH\rightarrow c\Gamma$ transitions are a factor $\sqrt{3}$ larger than those of $LH\rightarrow c\Gamma$ transitions. Therefore, in this polarization the OD value for $HH\rightarrow c\Gamma$ transitions is expected to be a factor of 3 larger than for $LH\rightarrow c\Gamma$ transitions. The low temperature absorption spectrum measured in the TE polarization, shown in Fig. 4, is consistent with this result. The OD at the energy of the $LH1\rightarrow c\Gamma 1$ transition is expected to be proportional to the sum of the square of the dipole matrix elements of the HH1-$c\Gamma$1 and LH1-$c\Gamma$1 transitions (d_{HH1} and d_{LH1}, respectively), because the LH1-$c\Gamma$1 absorption should be added to the HH1-$c\Gamma$1 absorption. Thus, within the approximations outlined in the final part of Sec. III, the expected ratio between the experimental LH1-$c\Gamma$1 and HH1-$c\Gamma$1 absorption peaks in TE mode can be estimated to be about $(d_{HH1}^2+d_{LH1}^2)/d_{HH1}^2=1.33$ and this value compares favorably with the experimental ratio of the LH1-$c\Gamma$1 and HH1-$c\Gamma$1 absorption peaks, which is about 1.20, despite the fact that the experimental ratio also includes excitonic effects, which are not considered in the elementary calculation of the dipole matrix. The agreement between the values of the calculated and the experimental peak absorption coefficients is also good: the slight energy difference between theoretical and experimental results for the peak positions is essentially due to the joint action of inhomogeneous strain effects and uncertainties in band alignment and excitonic binding energies (see Ref. 23 and references therein). Considering that only the Ge QW regions absorb, and taking into account the optical path schematically shown in Fig. 1(a), from the OD values of the HH1-$c\Gamma$1 transition it is possible to estimate an absorption coefficient $\alpha^{TE}=4.9\times10^3$ cm^{-1} for the TE polarization and $\alpha^{TM}=2.1\times10^3$ cm^{-1} for the TM polarization: both values agree very well with the tight-binding absorption coefficients $\alpha^{TE}=5.7\times10^3$ cm^{-1} and $\alpha^{TM}=2.3\times10^3$ cm^{-1}. These values are comparable with those characterizing MQWs based on III-V semiconductors.[34]

V. CONCLUSION

In conclusion, we have analyzed, through transmission measurements and theoretical calculations, the polarization dependence of the absorption spectra of strain balanced Ge/SiGe MQWs. Due to the close proximity of the direct and indirect gaps of bulk Ge, these structures are characterized by optical properties analogous to those of QWs based on direct gap III-V semiconductors. A simple geometry has been adopted for measuring the transmission of light polarized either parallel or nearly perpendicular to the QW plane. In this way, the optical anisotropy of the structure has been studied. The anisotropic absorption of light has been discussed in terms of electronic states and selection rules of type I direct gap quantum confined systems.

The good agreement between experimental data and theoretically predicted spectra, with respect to not only the transition energy but also the absorption coefficient value in both polarizations, confirms the effectiveness of the tight-binding model in describing the electronic states in SiGe heterostructures. These results have potential applications in polarization sensitive devices.

ACKNOWLEDGMENTS

The authors gratefully acknowledge the CARIPLO Foundation for the financial support through the SIMBAD Project and Stefan Stulz for sample processing.

*matteo.bonfanti@mater.unimib.it

[1] D. C. Houghton, G. C. Aers, S. R. Eric Yang, E. Wang, and N. L. Rowell, Phys. Rev. Lett. **75**, 866 (1995).
[2] Y. Miyake, J. Y. Kim, Y. Shiraki, and S. Fukatsu, Appl. Phys. Lett. **68**, 2097 (1996).
[3] M. L. W. Thewalt, D. A. Harrison, C. F. Reinhart, J. A. Wolk, and H. Lafontaine, Phys. Rev. Lett. **79**, 269 (1997).
[4] J. C. Sturm, H. Manoharan, L. C. Lenchyshyn, M. L. W. Thewalt, N. L. Rowell, J.-P. Noël, and D. C. Houghton, Phys. Rev. Lett. **66**, 1362 (1991).
[5] S. Fukatsu, H. Yoshida, N. Usami, A. Fujiwara, Y. Takahashi, Y. Shiraki, and R. Ito, Jpn. J. Appl. Phys., Part 2 **31**, L1319 (1992).
[6] N. L. Rowell, G. C. Aers, H. Lafontaine, and R. L. Williams, Thin Solid Films **321**, 158 (1998).
[7] D. J. Lockwood, J.-M. Baribeau, B. V. Kamenev, E.-K. Lee, and L. Tsybeskov, Semicond. Sci. Technol. **23**, 064003 (2008).
[8] F. Schäffler, Semicond. Sci. Technol. **12**, 1515 (1997).
[9] C. Rosenblad, H. von Känel, M. Kummer, A. Dommann, and E. Müller, Appl. Phys. Lett. **76**, 427 (2000).
[10] H. von Känel, M. Kummer, G. Isella, E. Müller, and T. Hackbarth, Appl. Phys. Lett. **80**, 2922 (2002).
[11] M. Bonfanti, E. Grilli, M. Guzzi, M. Virgilio, G. Grosso, D. Chrastina, G. Isella, H. von Känel, and A. Neels, Phys. Rev. B **78**, 041407(R) (2008).
[12] B. Rössner, D. Chrastina, G. Isella, and H. von Känel, Appl. Phys. Lett. **84**, 3058 (2004).
[13] *Numerical Data and Functional Relationships in Science and Technology*, edited by O. Madelung, Landolt-Börnstein, New Series, Group III, Vol. 17, Pt. A (Springer-Verlag, Berlin, 1982).
[14] S. Tsujino, H. Sigg, M. Scheinert, D. Grützmacher, and J. Faist, IEEE J. Sel. Top. Quantum Electron. **12**, 1642 (2006).
[15] K. Driscoll and R. Paiella, Appl. Phys. Lett. **89**, 191110 (2006).
[16] Y.-H. Kuo, Y. K. Lee, Y. Ge, S. Ren, J. E. Roth, T. I. Kamins, D. A. B. Miller, and J. S. Harris, Nature (London) **437**, 1334 (2005).
[17] W. H. Lau, V. Sih, N. P. Stern, R. C. Myers, D. A. Buell, A. C. Gossard, and D. D. Awschalom, Appl. Phys. Lett. **89**, 142104 (2006).

[18] H. Kosaka, H. Shigyou, Y. Mitsumori, Y. Rikitake, H. Imamura, T. Kutsuwa, K. Arai, and K. Edamatsu, Phys. Rev. Lett. **100**, 096602 (2008).
[19] D. A. B. Miller, D. S. Chemla, T. C. Damen, A. C. Gossard, W. Wiegmann, T. H. Wood, and C. A. Burrus, Phys. Rev. Lett. **53**, 2173 (1984).
[20] S. Tsujino, H. Sigg, G. Mussler, D. Chrastina, and H. von Känel, Appl. Phys. Lett. **89**, 262119 (2006).
[21] M. Bonfanti, E. Grilli, M. Guzzi, D. Chrastina, G. Isella, H. von Känel and H. Sigg, Physica E (Amsterdam) (to be published).
[22] D. Chrastina, A. Neels, M. Bonfanti, M. Virgilio, G. Isella, E. Grilli, M. Guzzi, G. Grosso, H. Sigg, and H. von Känel, Proceedings of the IEEE Fifth International Conference on Group IV Photonics, 2008, p. 194.
[23] M. Virgilio and G. Grosso, Phys. Rev. B **77**, 165315 (2008).
[24] J. S. Weiner, D. S. Chemla, D. A. B. Miller, H. A. Haus, A. C. Gossard, W. Wiegmann, and C. A. Burrus, Appl. Phys. Lett. **47**, 664 (1985).
[25] J.-Y. Marzin, M. N. Charasse, and B. Sermage, Phys. Rev. B **31**, 8298 (1985).
[26] I. Gontijo, G. Tessier, M. Livingstone, I. Galbraith, and A. C. Walker, Appl. Phys. Lett. **80**, 4027 (1996).
[27] J. Humlíček, A. Röseler, T. Zettler, M. G. Kekoua, and E. V. Khoutsishvili, Appl. Opt. **31**, 90 (1992).
[28] J.-M. Jancu, R. Scholz, F. Beltram, and F. Bassani, Phys. Rev. B **57**, 6493 (1998).
[29] C. G. Van de Walle and R. M. Martin, Phys. Rev. B **34**, 5621 (1986).
[30] M. Virgilio, R. Farchioni, and G. Grosso, Phys. Rev. B **71**, 155302 (2005).
[31] H. Haug and S. W. Koch, *Quantum Theory of the Optical and Electronic Properties of Semiconductors* (World Scientific, Singapore, 2004).
[32] G. Bastard, *Wave Mechanics Applied to Semiconductor Heterostructures* (Les Editions de Physique, Les Ulis, 1988).
[33] T. Fromherz, E. Koppensteiner, M. Helm, G. Bauer, J. F. Nützel, and G. Abstreiter, Phys. Rev. B **50**, 15073 (1994).
[34] W. T. Masselink, P. J. Pearah, J. Klem, C. K. Peng, H. Morkoç, G. D. Sanders, and Y.-C. Chang, Phys. Rev. B **32**, 8027 (1985).